

Kinetic simulations of collisionless magnetic reconnection in presence of a guide field

Paolo Ricci ^(1,2), J.U. Brackbill ⁽³⁾, W. Daughton ⁽³⁾, Giovanni Lapenta ^(1,3)

1) Istituto Nazionale per la Fisica della Materia (INFN) Politecnico di Torino, Torino, Italy 2) Dipartimento di Energetica, Politecnico di Torino, Torino, Italy 3) Los Alamos National Laboratory, Los Alamos, NM

arXiv:astro-ph/0304224v2 5 Dec 2003

P. Ricci, Dipartimento di Energetica, Politecnico di Torino, C.so Duca degli Abruzzi 24 - 10129 Torino, Italy.

J.U. Brackbill, W. Daughton, G. Lapenta, Los Alamos National Laboratory, Los Alamos NM 85745 (jub@lanl.gov, daughton@lanl.gov, lapenta@lanl.gov).

Abstract. The results of kinetic simulations of magnetic reconnection in Harris current sheets are analyzed. A range of guide fields is considered to study reconnection in plasmas characterized by different β values, $\beta > m_e/m_i$. Both an implicit Particle-in-Cell (PIC) simulation method and a parallel explicit PIC code are used. Simulations with mass ratios up to the physical value are performed. The simulations show that the reconnection rate decreases with the guide field and depends weakly on the mass ratio. The off-diagonal components of the electron pressure tensor break the frozen-in condition, even in low β plasmas. In high β plasmas, evidence is presented that whistler waves play a key role in the enhanced reconnection, while in low β plasmas the kinetic Alfvén waves are important. The in-plane and the out-of-plane ion and electron motion are also considered, showing that they are influenced by the mass ratio and the plasma β .

1. Introduction

Magnetic reconnection causes global changes of the magnetic field topology and of the plasma properties, and the conversion of magnetic energy into plasma particle kinetic energy in form of plasma jetting and plasma heating [*Biskamp*, 2000; *Priest and Forbes*, 2000].

Magnetic reconnection is observed to occur in collisionless plasmas over a wide range of β values: In the geomagnetic tail [*Øieroset*, 2001], $\beta \gg 1$; in the Earth's magnetopause [*Nishida*, 1978], $\beta \approx 1$; in the solar corona [*Priest*, 1982], in laboratory [*Gekelman et al.*, 1991; *Yamada* 1999; *Egedal et al.*, 2001; *Furno et al.*, 2003] and fusion plasmas [*Taylor*, 1986], in extragalactic jets [*Romanova and Lovelace*, 1992; *Blackman*, 1996], and in flares in active galactic nuclei [*Lesch and Birk*, 1997], $\beta \leq 1$.

In the high β case with zero guide field, the Geospace Environment Magnetic (GEM) reconnection challenge [*Birn et al.*, 2001; and references therein] has clarified the physics of fast reconnection. The primary mechanism by which the frozen-in condition is broken is given by the non-gyrotropic electron pressure terms [e.g., *Hesse et al.*, 1999; *Pritchett*, 2001; *Ricci et al.*, 2002b]. The reconnection rate is then enhanced thanks to the Hall term, which gives rise to the whistler dynamics and decouples the electron and ion motion [e.g., *Birn et al.*, 2001].

At lower β , the physics of fast reconnection plasmas is still under investigation. Theoretical [e.g., *Pritchett*, 2001] and experimental [*Yamada et al.*, 1997] results provide strong evidence that fast reconnection still occurs in lower β plasmas, but the reconnection rate is reduced. However, the scaling of the reconnection rate with the plasma β and with the mass ratio has not been clarified completely. Theoretical studies [*Kleva et al.*, 1995;

[*Biskamp, 1997; Rogers et al., 2001*] have proposed Kinetic Alfvén Wave (KAW) dynamics as the mechanism that enables fast reconnection in lower β plasmas, but the signature for this mechanism has been observed only in fluid simulations [*Rogers et al., 2003*]. Recently, for $\beta \approx 1$ plasmas, evidence has been presented that the off-diagonal terms of the electron pressure tensor break the frozen-in condition [*Hesse et al., 2002; Yin and Winske, 2003*] but it is not known what happens in lower β plasmas. The guide field allows drift motions that are responsible for a typical asymmetry in the ion and electron motion in the reconnection plane [*Hoshino and Nishida, 1983; Hoshino, 1987; Pritchett, 2001; Yin and Winske, 2003*] and the out-of-plane velocity is also affected by the plasma β [*Larrabee et al., 2003; Nodes et al., 2003*; and references therein], but how the velocities depend on the mass ratio and plasma β has not been examined.

The aim of the present paper is to study magnetic reconnection in plasmas with different β values, using kinetic simulation to study reconnection at low plasma β with mass ratios up to the physical value. The reconnection process is simulated using two Particle-in-Cell (PIC) codes, which model both kinetic ions and electrons. We use CELESTE3D, an implicit PIC code [*Brackbill and Forslund, 1985; Vu and Brackbill, 1992; Ricci et al., 2002a*], which is particularly suitable for large scale simulations with high mass ratios, and NPIC, a two-dimensional massively parallel explicit code [*Morse and Nielson, 1971; Forslund, 1985*], which is particularly suitable for studies of microphysical processes on all scales. The initial condition is a perturbed Harris sheet equilibrium and the system is permitted to evolve freely. The plasma β is changed by varying the intensity of the initial guide field, ranging from $\beta \gg 1$ (no guide field case), to $\beta < 1$ (strong guide field).

It should be remarked that other physical systems have been considered in the literature in order to study reconnection in low β plasmas [*Bobrova et al.*, 2001; *Nishimura et al.*, 2003; *Drake et al.*, 2003; *Rogers et al.*, 2003]. In *Nishimura et al.* [2003] a sheet pinch equilibrium is considered, and the growth of the tearing and Buneman instabilities are analyzed. In *Drake et al.* [2003] a double current layer is studied with $\lambda = 0.25d_i$, with total magnetic field B and density constant. The three-dimensional particle simulations performed therein show the development of turbulence which collapses in structures where the electron density is depleted. *Rogers et al.* [2003] consider fluid simulations of current layers of width $\lambda = d_i$ and point out that both the total β and the β based on the reconnecting field ($\beta_x = 8\pi n_0(T_i + T_e)/B_{x0}^2$) play an important role in determining the structure of the out-of-plane field and pressure profiles (in our simulation the total β is varied, while β_x is being held fixed). The conclusions described in the literature above do not apply directly to our results because they are based on a different equilibrium.

The primary mechanism that allows the break-up of the frozen-in condition and allows reconnection to proceed is analyzed in detail. The focus is on the presence of a strong guide field and its effect on the breaking of the frozen-in constraint. The guide field influence on the electron and ion motion is studied. The mechanism which permits fast reconnection in the presence of a guide field is studied; in particular, the simulations yield several new results. First, the dynamics of fast reconnection in the presence of a large guide field and high mass ratio is explored, resulting in the scaling of the reconnection rate with both of these parameters. Second, the simulations provide results on the break-up mechanism of the frozen-in condition in the presence of a strong guide field, a crucial problem in the physics of reconnection. Third, the influence of the guide field on the in-plane and out-of-

plane ion and electron velocities is analyzed. Finally, the physics of fast reconnection is discussed, showing for the first time in a fully kinetic simulation with a strong guide field the typical electron density pattern related to the KAW dynamics previously predicted by theoretical studies [*Kleva et al.*, 1995] and shown by fluid simulations [*Rogers et al.*, 2003].

The paper is organized as follows. Section II describes the physical problem and the numerical approach. Section III presents the results of the simulations, studies the mechanism for reconnection, analyzes the motion of ions and electrons, and examines the scaling of the reconnection rate with the mass ratio and the guide field.

2. Physical system and simulation approach

A Harris current sheet is considered in the (x, z) plane [*Harris*, 1962], with an initial magnetic field given by

$$\mathbf{B}_0(z) = B_0 \tanh(z/\lambda) \mathbf{e}_x + B_{y0} \mathbf{e}_y \quad (1)$$

and a plasma density given by

$$n_0(z) = n_0 \operatorname{sech}^2(z/\lambda) + n_b \quad (2)$$

The GEM physical parameters are used [*Birn et al.*, 2001]. The temperature ratio is $T_e/T_i = 0.2$, the current sheet thickness is $\lambda = 0.5d_i$, the background density is $n_b = 0.2n_0$, and the ion drift velocity in the y direction is $V_{i0} = 1.67V_A$, where V_A is the Alfvén velocity defined with the density n_0 and the field B_0 , and $V_{e0}/V_{i0} = -T_{e0}/T_{i0}$. The ion inertial length, $d_i = c/\omega_{pi}$, is defined using the density n_0 . The standard GEM challenge is modified by introducing an initially uniform guide field $B_y = B_{y0}$, which eliminates the line of null magnetic field. Different mass ratios are used, ranging from $m_i/m_e = 25$

(standard GEM mass ratio) to the physical mass ratio for hydrogen, $m_i/m_e = 1836$.

Following *Birn et al.* [2001], the Harris equilibrium is modified by introducing an initial flux perturbation in the form

$$A_y = -A_{y0} \cos(2\pi x/L_x) \cos(\pi z/L_z) \quad (3)$$

with $A_{y0} = 0.1B_0c/\omega_{pi}$.

The boundary conditions for the particles and fields are periodic in the x direction. Conducting boundary conditions are imposed for the fields at the z boundaries while reflecting boundary conditions are used for the particles.

The simulations shown in the present paper are performed using two PIC codes. CELESTE3D, an implicit PIC code, solves the full set of Maxwell-Vlasov equations using the implicit moment method [*Brackbill and Forslund, 1985; Vu and Brackbill, 1992; Ricci et al., 2002a*]. Maxwell's equations are discretized implicitly in time, as

$$\begin{cases} \nabla \cdot \mathbf{E}^\theta = 4\pi n^\theta \\ \nabla \times \mathbf{E}^\theta = -\frac{1}{c} \frac{\mathbf{B}^1 - \mathbf{B}^0}{\Delta t} \\ \nabla \cdot \mathbf{B}^1 = 0 \\ \nabla \times \mathbf{B}^\theta = \frac{1}{c} \frac{\mathbf{E}^1 - \mathbf{E}^0}{\Delta t} + \frac{4\pi}{c} \mathbf{J}^{1/2} \end{cases} \quad (4)$$

where the superscript 1 and 0 denote the new and old time levels, and $\theta \in [1/2, 1]$.

Newton's equations for each particle are also discretized implicitly in time:

$$\begin{cases} \mathbf{x}_p^1 = \mathbf{x}_p^0 + \mathbf{u}_p^{1/2} \Delta t \\ \mathbf{u}_p^1 = \mathbf{u}_p^0 + \frac{q_s \Delta t}{m_s} \left[\mathbf{E}^\theta(\mathbf{x}_p^{1/2}) + \frac{\mathbf{u}_p^{1/2} \times \mathbf{B}^0}{c} \right] \end{cases} \quad (5)$$

The implicit moment method allows more rapid simulations on ion length and time scales than explicit methods, while retaining the kinetic effects of both electrons and ions. The explicit simulation must observe the time step limit, $\Delta t < 2/\omega_{pe}$, and the mesh spacing required to avoid the finite grid instability, $\Delta x \leq 2\lambda_{De}$, with ω_{pe} and λ_{De} denoting

the electron frequency and the electron Debye length. These two constraints are replaced in implicit simulations by an accuracy condition, $v_{th,e}\Delta t < \Delta x$, whose principal effect is to determine how well energy is conserved. In general, the accuracy condition permits much larger Δx and Δt than possible with explicit methods.

The explicit plasma simulation code NPIC is based on a well-known explicit electromagnetic algorithm [*Morse and Nielson, 1971; Forslund, 1985*]. In this full-Maxwell approach, the fields are advanced using the scalar and vector potentials. Working in the Coulomb gauge, the scalar potential is computed directly from Poisson's equation, while the vector potential is advanced in time using either a simple explicit algorithm [*Morse and Nielson, 1971*] or a semi-implicit method that permits the time step to exceed the Courant limit [*Forslund, 1985*]. Intuitively, this corresponds to an implicit treatment of light waves, while the rest of the algorithm remains explicit and the electron plasma frequency and cyclotron motion are fully resolved. In this manuscript, all simulations at low mass ratio $m_i/m_e = 25$ were performed with the simple explicit version of the field solver, while two of the simulations at higher mass ratio ($m_i/m_e = 180$, $B_{y0} = 0$, B_0) were performed with the semi-implicit version of the field solver with a time step approximately three times larger than the Courant limit. For the strong guide field high mass ratio case ($m_i/m_e = 180$, $B_{y0} = 5B_0$), the simple explicit field solver was employed since the time constraint imposed by the guide field on the particle mover is more limiting. Extensive comparisons between the two versions of the field solver have revealed no significant differences. The particle trajectories within NPIC are advanced using the leapfrog technique, and particle moments are accumulated with area weighting. To run on a parallel computer, the code is written using domain decomposition with calls to the MPI library.

The implicit PIC method, and particularly the code CELESTE3D, has been applied to many problems in plasma physics in one dimension [*Lapenta and Brackbill, 1994; Lapenta, 2002*], in two dimensions [*Quest et al., 1983; Forsslund et al., 1984; Dreher et al., 1996; Lapenta and Brackbill, 1997; Lapenta and Brackbill, 2002; Ricci et al., 2002a; Ricci et al., 2002b; Lapenta et al., 2003*], and in three dimensions [*Lapenta and Brackbill, 2000; Lapenta et al., 2003*]. NPIC has been used to study the dynamics of thin current layers [*Daughton, 2002; Daughton, 2003*]

Implicit PIC methods are particularly suitable when simulating systems with higher mass ratios. The cost of an explicit simulation on ion time and space scales varies with the ion to electron mass ratio as $(m_i/m_e)^{(d+2)/2}$, where d is the number of spatial dimensions [*Pritchett, 2000*]. For example, in two dimensions, a simulation of the GEM challenge with $m_i/m_e = 1836$ is more than 5000 times as expensive as one with $m_i/m_e = 25$ if the explicit method is used. In contrast, the cost of an implicit simulation scales as $(m_i/m_e)^{1/2}$, as the time step can be kept constant with respect to the ion plasma frequency and the ratio ω_{ci}/ω_{pi} is scaled as $(m_i/m_e)^{1/2}$, in order to maintain the same Harris sheet equilibrium [*Ricci et al., 2002b*]. (The ratio $v_{th,e}/c$ is kept constant while v_A/c is decreased when the mass ratio is increased). The explicit PIC method resolves all relevant scales within the plasma, and with a massively parallel computer, high mass ratio simulations are now quite feasible in two dimensions. In the present work, the explicit simulations are run on a machine using as many as 128 nodes.

The simulations have been performed by the two codes with remarkably different simulation parameters. With $m_i/m_e = 25$, CELESTE3D uses a $N_x \times N_z = 64 \times 64$ grid, with time step $\omega_{pi}\Delta t = 0.3$, and 25 particles per species per cell, for a total of $2 \cdot 10^5$

computational particles. The high mass ratio simulations are performed by CELESTE3D with the same simulation parameters, except for the $m_i/m_e = 1836$ case where the time step is reduced to $\omega_{pi}\Delta t = 0.1$. With $m_i/m_e = 25$, NPIC employs a $N_x \times N_z = 1024 \times 512$ grid, $104 \cdot 10^6$ computational particles and a time step corresponding to $\omega_{pi}\Delta t = 0.029$ for $B_{y0} = 0, B_0$, and $\omega_{pi}\Delta t = 0.014$ at $B_{y0} = 5B_0$. For the high mass ratio cases $m_i/m_e = 180$, the simulation parameters are $N_x \times N_z = 2560 \times 1280$, $1 \cdot 10^9$ particles, and a time step $\omega_{pi}\Delta t = 0.019$ for $B_{y0} = 0, B_0$, and $\omega_{pi}\Delta t = 0.0064$ at $B_{y0} = 5B_0$.

The reconnected fluxes for mass ratios 25 and 180 from the two codes show a remarkable agreement. A detailed comparison of the electron dynamics for $m_i/m_e = 25$ has been performed, which shows that the physical mechanisms revealed by the two codes agree, although CELESTE3D does not resolve all the electron scales. In fact, it is important to note that even at the mass ratio 25, the CELESTE3D grid does not resolve the electron scales; in particular, the electron Debye length λ_e , the electron skin depth $d_e = c/\omega_{pe}$, the electron gyroradius ρ_e , and ρ_s ($\rho_s^2 = c^2 m_i T_e / e^2 B_{y0}^2$) are not resolved.

Certainly, the accuracy of wave-particle interactions on the fast time scale is reduced using a coarser grid and a bigger time step. However, results of the simulations shown here and many previous simulations show that kinetic electrons seem to contribute correctly on the ion time scales: Generally speaking, kinetic electrons contribute inertial effects, anisotropic pressure, and electron thermal transport on the ion time scales that would otherwise have to be modelled if fluid electron equations were used [*Forslund and Brackbill, 1982; Brackbill et al., 1984; Vu and Brackbill, 1993; Lapenta and Brackbill, 1996; Ricci et al., 2002b*].

Convergence studies of the implicit PIC method have already been presented in *Brackbill and Forslund* [1985] and *Brackbill and Vu* [1991]. The non-linear evolution of the LHDI predicted by CELESTE3D [*Lapenta and Brackbill*, 2002], has been confirmed by explicit results [*Lapenta et al.*, 2003]. Regarding the GEM challenge, it has already been shown that results with CELESTE3D are comparable in detail with those of explicit simulations [*Pritchett*, 2000] for $m_i/m_e = 25$ and $B_{y0} = 0$ [*Ricci et al.*, 2002a]. A convergence study in presence of a guide field has been performed. In Tab. I, the dependence of conservation of the total energy of the plasma on the time step is studied for $B_{y0} = 5B_0$ and $m_i/m_e = 25$. For reference, the energy conservation for the explicit method is also shown.

3. Simulation results

A set of simulations is performed, using different mass ratios ($m_i/m_e = 25$, $m_i/m_e = 180$, and $m_i/m_e = 1836$) and different guide fields: the standard GEM challenge with $B_{y0} = 0$, $B_{y0} = B_0$ and $B_{y0} = 5B_0$, corresponding to $\beta = \infty$, $\beta = 1.2$, and $\beta = 0.048$, in the center of the current sheet [$\beta = 8\pi n_0(T_i + T_e)/(B_{y0}^2)$].

In all cases, the typical evolution of the magnetic flux and the out-of-plane current is similar to the picture of magnetic reconnection in the absence of a guide field provided by the GEM challenge project [e.g., *Ricci et al.*, 2002a]. In particular, in the presence of a guide field reconnection still occurs but it requires a longer time and saturates at a lower level. The current is considerably more filamentary and peaks of negative current appear which are not present in the standard GEM challenge with no guide field.

In Fig. 1, the reconnection rates for both NPIC and CELESTE3D simulations are shown. The reconnected flux is measured as the flux difference, $\Delta\Psi$, between the X and the O points. All the simulations show a similar evolution. After slow initial growth,

which lasts until $t\omega_{ci} \approx 10$ (or longer, for higher guide fields), reconnection enters a fast phase that persists until the saturation level is reached. During the fast reconnection phase, both NPIC and CELESTE3D (when simulations with enhanced spatial resolution are performed) show multiple small scale islands, which merge at later time into a single island. In general, the reconnection rate decreases as the guide field increases for all values of the mass ratio. However, a fast reconnection phase is always present. The saturation level also decreases with the guide field, because the out-of-plane magnetic field influences the plasma motion reducing its compressibility. It is also shown that the reconnection rate depends weakly on the mass ratio for all the guide fields considered. Simulations are performed with $m_i/m_e = 25, 180, 1836$ with the implicit PIC code CELESTE3D and with $m_i/m_e = 25, 180$ for the explicit PIC code NPIC. For the reconnected flux, the results of the explicit and implicit simulations agree remarkably well for both mass ratios. In some cases, the fast reconnection phase starts earlier in implicit simulations; nevertheless, both the reconnection rate and the saturation level is similar in the two codes. The later start is probably due to the reduced initial noise in the explicit simulation because of much larger number of particles.

From an energetic point of view, the reconnection process causes a decrease of the total magnetic energy, because the x -component of the magnetic field is destroyed by the reconnection process. In particular our results show that, while the energy related to the y -component of the magnetic field is almost constant (it slightly increases in the $B_y = 0, B_0$ case), the B_x field energy decreases, and the energy of the z -component of the magnetic field, which is created during the reconnection process, grows. The lost magnetic energy is transferred to the ions and electrons in form of kinetic energy.

In the following section, the mechanism which leads to the break-up of the frozen-in condition for electrons is analyzed, and the general motion of ions and electrons depending on the guide field is studied. Finally, the mechanism of fast reconnection is studied, when the whistler dynamics are suppressed by the presence of the guide field.

3.1. Break of the frozen-in condition

Ohm's law in collisionless plasmas states that the reconnection electric field, which is proportional to the reconnection rate, can be expressed as [e.g., *Pritchett*, 2001; *Ricci et al.*, 2002b]

$$\begin{aligned}
 E_{y,rec} = & -\frac{1}{c}(v_{ze}B_x - v_{xe}B_z) - \frac{1}{en_e}\left(\frac{\partial P_{xye}}{\partial x} + \frac{\partial P_{yze}}{\partial z}\right) \\
 & - \frac{m_e}{e}\left(\frac{\partial v_{ye}}{\partial t} + v_{xe}\frac{\partial v_{ye}}{\partial x} + v_{ze}\frac{\partial v_{ye}}{\partial z}\right)
 \end{aligned} \tag{6}$$

At the X point, the magnetic field components B_x and B_z vanish and the only contributions to the reconnection electric field are given by gradients of the off-diagonal terms of the electron pressure or by the terms related to electron inertial effects.

In the zero guide field case, *Kuznetsova et al.* [2000] show that the electrons become demagnetized near the X point, at distances comparable to the electron meandering lengths,

$$d_{xe} = \left[\frac{c^2 m_e T_e}{e^2 (\partial B_z / \partial x)^2}\right]^{1/4}, \quad d_{ze} = \left[\frac{c^2 m_e T_e}{e^2 (\partial B_x / \partial z)^2}\right]^{1/4} \tag{7}$$

and execute a bounce motion which results in the presence of off-diagonal terms of the electron pressure tensor. In this case, the off-diagonal terms of the electron pressure are most important in breaking the frozen-in condition [*Pritchett*, 2001; *Ricci et al.*, 2002b]. In the presence of a weak guide field ($B_{y0} = 0.3B_0$, $B_{y0} = 0.8B_0$), evidence has been given that the electron pressure is still the mechanism that allows reconnection [*Hesse et al.*, 2002; *Yin and Winske*, 2003].

Figures 2 and 3 show the non-ideal part of out-of-plane electric field [i.e., $E_y + (v_{ze}B_x - v_{xe}B_z)/c$], which is the difference between the electric field E_y and the ideal terms $\mathbf{v}_e \times \mathbf{B}/c$], and the contribution of the electron pressure terms close to the X point during the reconnection process. Simulations performed by NPIC (Fig. 2) and CELESTE3D (Fig. 3) with the guide fields $B_{y0} = 0$, $B_{y0} = B_0$, and $B_{y0} = 5B_0$ are considered for a mass ratio $m_i/m_e = 25$.

In the $B_{y0} = 0$ case, the electron pressure tensor is the dominant contribution at the X point [e.g., *Pritchett*, 2001; *Ricci et al.*, 2002b] on a scale length of the order of the electron meandering length [*Ricci et al.*, 2002b]. NPIC and CELESTE3D results agree well, although NPIC results are more refined because of the higher number of particles.

For $B_{y0} = B_0$ and $B_{y0} = 5B_0$, the results of the two codes look less alike. Both NPIC and CELESTE3D do indicate that the contribution of the electron pressure tensor is responsible for the break-up of the frozen-in condition for all the guide fields. Moreover, the numerical value of the non-ideal electric field at the X point and its pressure contribution, which is equal to the reconnection rate, are similar in the explicit and implicit simulations. However, the higher resolution of NPIC reveals that the characteristic thickness of the break-up region is of the order of ρ_e in presence of a guide field. Nevertheless, CELESTE3D appears to capture the break-up region for the electrons.

The out-of-plane electron velocity evaluated from both simulations shows that electron inertia alone cannot be responsible for the break-up mechanism [*Hesse et al.*, 1999]. Thus, only the pressure terms can be relevant at the X point, and the implicit moment method spreads out the electron diffusion region from the electron gyroradius to a scale linked to the grid spacing.

As an aside, it should be noted that in the presence of a guide field the symmetry of the break-up region seen in the $B_{y0} = 0$ case is lost and is replaced by a more complex non-symmetric structure.

In Fig. 4, which shows results for the case $m_i/m_e = 25$ and $B_{y0} = 5$ from NPIC, allows to study the contributions to the non-ideal electric field (Fig. 4a). In Fig. 4b are shown the off-diagonal terms of the electron pressure tensor, in Fig. 4c the convective inertial terms, $v_{xe}\partial v_{ye}/\partial x + v_{ze}\partial v_{ye}/\partial z$, and in Fig. 4d the inertial term, computed as the difference between the non-ideal electric field and the pressure contribution. As in the zero guide field case, the pressure terms dominate in the region closest to the X point, while the inertia terms are relevant at intermediate lengths. The contribution of the term $\partial v_{ye}/\partial t$ appears small because Fig. 4c and Fig. 4d are similar. The ideal terms give the main contribution far away from the reconnection region. According to these results, the importance of the pressure terms does not decrease in presence of a guide field. However, the spatial thickness of the region in which these terms dominate is of order ρ_e and thus decreases with increasing guide field.

Figures 2-4 confirms the finding by Hesse *et al.* [2002] that the electron pressure is the dominant non-ideal term with $B_{y0} \approx B_0$, and extends it also to a plasma with lower β . As an aside, it should be pointed out that simulations with $B_{y0} = 5B_0$ that explore the electron break-up region are computationally very expensive, as they require the accurate resolution of the electron Larmor motion.

According to Hesse *et al.* [2002], the off-diagonal pressure is generated by gradients of the electron flow velocity in the y direction and by differences in the diagonal terms of

the pressure tensor, as [Hesse *et al.*, 2002]

$$P_{xye} = -\frac{P_{zze}}{\omega_{ce}} \frac{\partial v_{ye}}{\partial z} + \frac{B_x}{B_y} (P_{yye} - P_{zze}) \quad (8)$$

$$P_{yze} = -\frac{P_{xxe}}{\omega_{ce}} \frac{\partial v_{ye}}{\partial x} + \frac{B_z}{B_y} (P_{yye} - P_{xxe}) \quad (9)$$

where the heat flux has been ignored. It is assumed that $B_y \gg B_x$ and $B_y \gg B_z$, that the diagonal components of the pressure tensor are much larger than the off-diagonal components, and that $\tau \ll v_e/L$, where τ is a typical evolution scale, v_e is a typical electron velocity, and L is a typical scale length.

Hesse *et al.* [2002] show a good match between the anisotropies, estimated from Eqs. (8) and (9), and the values obtained directly from the simulations, for the $B_{y0} = 0.8B_0$ case. For the $B_{y0} = 5B_0$ case, Fig. 5 compares the actual value of P_{xye} and P_{yze} obtained from the simulation, with the value computed from Eqs. (8) and (9), for the NPIC simulation. Once again, there is a good agreement between the simulation results and the theoretical predictions. The contribution of $P_{zze}/\omega_{ce}\partial v_{ye}/\partial z$ is relevant in the evaluation of P_{xye} , while the contribution of $P_{xxe}/\omega_{ce}\partial v_{ye}/\partial x$ is unimportant to P_{yze} . CELESTE3D confirms these findings. The mechanism through which the differences among the diagonal terms of the electron pressure arises has been studied by Ricci *et al.* [2003] and can be extended to higher guide field.

The agreement between our results and Hesse *et al.* [2002] is two-fold. First, our simulations agree with the theoretical model of Eqs. (8) and (9). Second, our results obtained with NPIC and the implicit code CELESTE3D agree with the conclusions obtained by Hesse *et al.*'s code for $B_{y0} \approx B_0$. Furthermore, the conclusions by Hesse *et al.* [2002] are extended to larger guide fields, a parameter regime not yet explored.

3.2. Ion and electron motion

When $B_{y0} = 0$, the ions and electrons $\mathbf{E} \times \mathbf{B}$ drift towards the X point along the z direction (see e.g. Pritchett [2001]). The ions become demagnetized at distances of the order of a few d_i , because of the Hall effect, are accelerated along the y direction by the reconnection electric field, E_y , and flow outwards in the x direction at the Alfvén speed, where they are diverted by the B_z magnetic field. The electrons follow a similar flow pattern, except that they are demagnetized at shorter distances, of the order of the electron meandering lengths [see Eq. (7)], and are expelled at super-Alfvénic velocities. The whole ion and electron motion is up-down and left-right symmetric.

The presence of a guide field rotates the $\mathbf{E} \times \mathbf{B}$ motion, causes ions and electrons to drift in directions not otherwise possible [Yin and Winske, 2003], and destroys the symmetry with respect to the $z = 0$ axes. In Figs. 6-7, the ion and electron motion in the (x, z) plane is represented in the presence of a guide field.

In all cases, the ions are diverted when they approach the X point in an antisymmetric way with respect to the $x = 0$ line. Their outflow motion is primarily along x . The outflow region becomes smaller as the guide field increases. The electron dynamics are completely different and depend strongly on the guide field. In the $B_{y0} = B_0$ case (Fig. 6) electrons exhibit a strong flow along the separatrix. The motion is inward in the first and third quadrant, and outward in the second and fourth quadrants. Our simulation confirms the asymmetric motion of the electrons, which has been shown theoretically to have an important role in the reconnection process [Kleva *et al.*, 1995; Biskamp, 1997; Rogers *et al.*, 2001; Yin and Winske, 2003]. In the presence of a stronger guide field,

$B_{y0} = 5B_0$, (Fig. 7), the electrons flow with a similar pattern to the $B_{y0} = B_0$ case, but the in-plane motion is more localized.

The electron motion along the y direction (i.e., the out-of-plane direction of the guide field) is also affected by the guide field [*Horiuchi and Sato, 1997*]. This is shown in Fig. 8, where CELESTE3D and NPIC results are compared. When $B_{y0} = 0$, the ions are accelerated by the reconnection electric field, E_y , at the X point along the y direction. However, the B_z field diverts the electrons, decreasing the y velocity, and forcing the outflow in the x direction. In the presence of a guide field, even far from the X point, the electrons maintain a significant velocity in the y direction, as they flow along the magnetic field. The electron motion is concentrated at the separatrix and the y velocity increases with the guide field. CELESTE3D results [*Ricci et al, 2003*] reveal also a dependence of the out-of-plane velocity on the mass ratio, showing that lighter electrons reach higher velocities. This particle acceleration may have important consequences in active galactic nuclei, extragalactic jets, solar flares and auroral arcs [*Larrabee et al., 2003; Nodes et al., 2003* and references therein].

3.3. Fast reconnection mechanism

When $B_{y0} = 0$, the off-diagonal terms of the electron pressure provide the primary mechanism by which the electrons break the frozen-in condition, and the Hall term in Ohm's law decouples electron and ion motion and strongly enhances the reconnection rate. Because of the Hall effect, the electron and ion motion decouple at a distance of the order of d_i and the whistler dynamics are enabled. The whistler waves have a quadratic dispersion relation ($\omega \propto k^2$) [*Biskamp, 1997*], which allows fast reconnection, even when the diffusion region is small [*Shay et al., 2001*]. The typical signature of the Hall effect

is the presence of a quadrupolar out-of-plane magnetic field [Sonnerup, 1979; Terasawa, 1983] which has also been observed by some satellite observations [Øieroset *et al.*, 2001; Mozer *et al.*, 2002].

At low β , provided that $\beta > m_e/m_i$ (i.e., $\rho_s > d_e$, $\rho_s^2 = c^2 m_i (T_e + T_i) / e^2 B_{y0}^2$), it has been pointed out that the whistler dynamics are pushed to smaller scales [Rogers *et al.*, 2001], because of magnetic field compression, $B_{y0} \nabla \cdot \mathbf{v}$, which remains finite even if the motion is almost incompressible [Biskamp, 1997]. Nevertheless, due to the electron pressure term, and in particular the parallel gradient of the electron density, $\nabla_{\parallel} n_e$, KAW dynamics arise. The KAWs are characterized by a quadrupole density structure with a scale length ρ_s , which replaces d_i as the spatial scale of interest in presence of a guide field [Kleva *et al.*, 1995; Biskamp, 1997; Rogers *et al.*, 2001]. KAWs have the same dispersion properties as whistler waves ($\omega \propto k^2$) and enable fast reconnection [Biskamp, 1997]. At still lower β ($\beta < m_e/m_i$), ions and electrons are tightly coupled, ions are forced to follow the electron dynamics, and fast reconnection is not possible [Biskamp *et al.*, 1997; Ottaviani and Porcelli, 1993]. All of our simulations have a plasma β that permits fast reconnection. The mechanism for fast reconnection operative at various β have been explored with fluid model [Rogers *et al.*, 2003]. Here we present the first systematic kinetic study of fast reconnection mechanism as a function of the plasma β .

In Fig. 9, the out-of-plane magnetic field during the reconnection process is plotted for different mass ratios and different guide fields. In the zero guide field case, the out-of-plane magnetic field presents the typical quadrupolar symmetric structure due to the Hall effect [Sonnerup, 1979; Terasawa, 1983]. When a guide field is added to the initial Harris sheet equilibrium, the out-of-plane magnetic field is dramatically altered. The

quadrupolar structure due to the Hall effect, is weakened and tilted at $B_{y0} = B_0$, and is unidentifiable for $B_{y0} = 5B_0$. Even if the pattern of the magnetic field does not depend on the mass ratios, the maximum and minimum values are affected. The reason for this is the out-of-plane magnetic field depends on the in-plane current which is due to the decoupling of ion and electron motion and the electron motion depends on the mass ratio, influencing the out-of-plane magnetic field.

The width of the ion outflow region is shown in Fig. 10 for three different guide fields, by examining the x -component of the ion velocity, v_{xi} . It is remarkable that for all guide fields, the ion outflow pattern is not influenced by the mass ratios. It follows that, at least for the range of guide fields studied, there is a mechanism that decouples the ion and electron dynamics (the electron dynamics depend on the mass ratio). Without a guide field, the outflow region is of the order of a few d_i . In the presence of the guide field $B_{y0} = B_0$, the outflow width decreases, and the outflow region with $B_{y0} = 5B_0$ is narrower than with $B_{y0} = B_0$ case (Fig. 10). We note also that the scale length of interest, ρ_s , of this regime decreases when the guide field increases.

The electron density pattern in the presence of a guide field is plotted in Fig. 11. The quadrupolar pattern close to the reconnection region is predicted by theory [Kleva *et al.*, 1995], and it is a distinctive feature of the fast reconnection enabled by the KAW physics.

Table II summarizes the variation of the reconnection rates, with the guide field and mass ratio. The average growth rates are listed.

The reconnection rate decreases as the guide field increases and the fast reconnection mechanism transitions from whistler dynamics to KAW dynamics. Experimental results confirm this trend [Yamada *et al.*, 1997] as well as previous numerical results [Pritchett,

2001]. A scaling law for the reconnection rate has been proposed with this same property [Wang *et al.*, 2000]. Horiuchi and Sato [1999] propose another scaling law for the reconnection rate which shows a decrease of the reconnection rate as the guide field increases and which applies to driven reconnection.

The reconnection rate shows only a weak dependence on the mass ratio. For $B_{y0} = 0$, Shay and Drake [1998] have demonstrated that the reconnection rate is insensitive to the physics that breaks the frozen-in condition, as a consequence, is insensitive to the electron mass. This is confirmed by previous kinetic calculations [Pritchett, 2001] and extended to the physical mass ratio by Ricci *et al.* [2002b].

4. Conclusions

By performing kinetic simulations of Harris current sheets with different guide fields and different mass ratios, the physics of magnetic reconnection in plasmas characterized by different β values has been studied.

A main result of these simulations is the scaling of the reconnection rate with the guide field and the mass ratio, up to physical values. As in the case of high β plasmas, the mechanism which breaks the electron frozen-in condition is provided by the off-diagonal terms of the electron pressure tensor. The simulations extend the results to high guide fields, and demonstrate that the scale length of the diffusion region passes from the electron meandering length for $B_{y0} = 0$ to the electron gyroradius in presence of a guide field. The simulations indicate that the mechanism that allows fast reconnection changes with β . For high β , the typical quadrupolar structure of the out-of-plane magnetic field associated to the whistler dynamics whistler dynamics is present in the simulations. This mechanism allow the decoupling of electrons and ions. At low β (high guide fields), the KAW dynamics

allows the decoupling and, the quadrupolar electron density pattern which characterize the KAW and which had been predicted theoretically and by fluid models before is revealed by the simulations. The presence of a guide field causes additional components of the $\mathbf{E} \times \mathbf{B}$ drift, which modify the ion and electron motion causing asymmetric plasma flow.

The comparison between the implicit and the explicit codes has shown a remarkable agreement for phenomena occurring on spatial scales resolved by both codes (e.g., the reconnected flux, the structure of the out-of-plane magnetic field, the electron velocity). A phenomenon occurring on spatial scale not resolved by CELESTE3D, like the mechanism of the electron break-up mechanism, is still present in the implicit code, but its effect has been spread out to a more extended spatial scale.

In closing, we note that an experimental setup has been built to study experimentally the dependence of reconnection on the guide field [Furno *et al.*, 2003] and we plan to compare our simulation results with the experiments.

Acknowledgments. The authors gratefully acknowledge useful discussions with J. Birn, J. Egedal, P. Gary, R.V.E. Lovelace, M. Ottaviani, F. Porcelli, B.N. Rogers, M. Yamada, and L. Yin. This research is supported by the LDRD program at the Los Alamos National Laboratory, by the United States Department of Energy, under Contract No. W-7405-ENG-36 and by NASA, under the "Sun Earth Connection Theory Program".

References

Birn, J., et al., Geospace Environment Modelling (GEM) magnetic reconnection challenge, *J. Geophys. Res.*, 106, 3715, 2001.

Biskamp, D., Magnetic reconnection in plasmas, Cambridge University Press (Cambridge, New York, 2000).

Biskamp, D., Collisional and collisionless magnetic reconnection, *Phys. Plasmas*, *4*, 1964, 1997.

Biskamp, D., E. Schwarz, J.F. Drake, Two-fluid theory of collisionless magnetic reconnection, *Phys. Plasmas*, *4*, 1002, 1997.

Blackman, E.G., Reconnecting magnetic flux tubes as a source of in situ acceleration in extragalactic radio sources, *Astrophys. J. Lett.*, *456*, LT87, 1996.

Bobrova, N.A., S.V. Bulanov, J.I. Sakai, and D. Sugiyama, Force-free equilibria and reconnection of the magnetic field lines in collisionless plasma configurations, *Phys. Plasmas*, *8*, 759, 2001.

Brackbill, J. U., D. W. Forslund, K. B. Quest, and D. Winske, Nonlinear evolution of the lower-hybrid drift instability, *Phys. Fluids*, *27*, 2682, 1984.

Brackbill, J. U. and D. W. Forslund, Simulation of low frequency, electromagnetic phenomena in plasmas, in *Multiple Times Scales*, J.U. Brackbill and B.I. Cohen Eds., (Accademic Press, Orlando, 1985), pp. 271-310.

Daughton, W., Nonlinear dynamics of thin current sheets, *Phys. Plasmas*, *9*, 3668, 2002.

Daughton, W., Electromagnetic properties of the lower-hybrid drift instability in a thin current sheet, *Phys. Plasmas*, *10*, 3103, 2003.

Drake, J.F., M. Swisdak, C. Cattell, M.A. Shay, B.N. Rogers, A. Zeiler, Formation of electron holes and particle energization during magnetic reconnection, *Science*, *299*, 873 (2003).

Dreher, J., U. Arendt, and K. Schindler, Particle simulations in collisionless reconnection in magnetotail configuration including electron dynamics, *J. Geophys. Res.*, *101*, 27375 (1996).

Forslund, D. W. and J. U. Brackbill, Magnetic-field induced surface transport on laser-irradiated foils, *Phys. Rev. Lett.*, *48*, 1614, 1982.

Forslund, D.W., K.B. Quest, J.U. Brackbill, and K. Lee, Collisionless dissipation in quasi-perpendicular shocks, *J. Geophys. Res.*, *89*, 2142, 1984.

Forslund, D., Fundamentals of Plasma Simulation, *Space Science Reviews*, *42*, 3, 1985.

Furno, I., T. Intrator, E. Torbert, C. Carey, M. D. Cash, J. K. Campbell, W. J. Fienup, C. A. Werley, G. A. Wurden, and G. Fiksel, Reconnection Scaling Experiment: a new device for three dimensional magnetic reconnection studies, *Rev. Sci. Instrum.*, *74*, 2324, 2003.

Gekelman, W., H. Pfister, Z. Lucky, J. Bamber, D. Leneman, and J. Maggs, Design, construction, and properties of the large plasma research device - the LAPD at UCLA, *Rev. Sci. Instrum.*, *62*, 2875, 1991.

Harris, E.G., On a plasma sheath separating regions of oppositely directed fields, *Nuovo Cimento Soc. Ital. fis. A-D*, *23*, 115, 1962.

Hesse, M., K. Schindler, J. Birn, and M. Kuznetsova, *The diffusion region in collisionless magnetic reconnection*, *Phys. Plasmas*, *6*, 1781, 1999.

Hesse, M., M. Kuznetsova, and M. Hoshino, The structure of the dissipation region for component reconnection: Particle simulations, *Geophys. Res. Lett.*, *29*, 2001GL014714, 2002.

Horiuchi, R., and T. Sato, Particle simulation study of collisionless driven reconnection in sheared magnetic field, *Phys. Plasmas*, *4*, 277, 1997.

Hoshino, M., and A. Nishida, Numerical simulation of the dayside reconnection, *J. Geophys. Res.*, *88*, 6926, 1983.

Hoshino, M., Electrostatic effect for collisionless tearing mode, *J. Geophys. Res.*, *92*, 7368, 1987.

Kleva, R.G., J.F. Drake, and F.L. Waelbroeck, Fast reconnection in high temperature plasmas, *Phys. Plasmas*, *2*, 23, 1995.

Kuznetsova, M.M., M. Hesse, and D. Winske, Toward a transport model of collisionless magnetic reconnection, *J. Geophys. Res.*, *105*, 7601, 2000.

Lapenta, G., and J.U. Brackbill, Dynamic and selective control of the number of particles in kinetic plasma simulations, *J. Comp. Phys.*, *115*, 213, 1994.

Lapenta, G., and J.U. Brackbill, Contact discontinuities in collisionless plasmas: a comparison of hybrid and kinetic simulation, *Geophys. Res. Lett.*, *23*, 1713, 1996.

Lapenta, G., and J.U. Brackbill, A kinetic theory for the drift-kink instability, *J. Geophys. Res.*, *102*, 27099, 1997.

Lapenta, G., and J. U. Brackbill, 3D reconnection due to oblique modes: a simulation of Harris current sheets, *Nonlinear Processes Geophys.*, *7*, 151, 2000.

Lapenta, G., Particle rezoning for multidimensional kinetic particle-in-cell simulations, *J. Comp. Phys.*, *181*, 317, 2002.

Lapenta, G., and J.U. Brackbill, Nonlinear evolution of the lower hybrid drift instability: Current sheet thinning and kinking, *Phys. Plasmas*, *9*, 1544, 2002.

Lapenta, G., J.U. Brackbill, and W. Daughton, The unexpected role of the lower hybrid drift instability in magnetic reconnection in three dimensions, *Phys. Plasmas*, *10*, 1577, 2003.

Larrabee, D.A., R.V.E. Lovelace, and M.M. Romanova, Lepton acceleration by relativistic collisionless magnetic reconnection, *Astrophys. J.*, *586*, 72, 2003.

Lesch, H. and G.T. Birk, Particle acceleration by magnetic field-aligned electric fields in active galactic nuclei, *Astron. Astrophys.*, *324*, 461, 1997.

Morse, R., and C. Nielson, Numerical simulation of Weibel instability in one and two dimensions, *Phys. Fluids*, *14*, 830, 1971.

Mozer, F.S., S.D. Bale, and T.D. Phan, Evidence of diffusion regions at the subsolar magnetopause crossing, *Phys. Rev. Lett.*, *89*, 015002, 2002.

Nishidam, A., *Geomagnetic Diagnostics of the Magnetosphere* (Springer-Verlag, New York, 1978).

Nishimura, K., S.P. Gary, H. Li, S.A. Colgate, Magnetic reconnection in a force-free plasma: Simulations of micro- and macro instabilities, *Phys. Plasmas*, *10*, 347 (2002).

Nodes C., G.T. Birk, H. Lesch, and R. Schopper, Particle acceleration in three-dimensional tearing configuration, *Phys. Plasmas*, *10*, 835, 2003.

Øieroset, M., T.D. Phan, M. Fujimoto, R.P. Lin, and R.P. Lepping, In situ detection of collisionless reconnection in the Earth's Magnetotail, *Nature*, *412*, 414, 2001.

Ottaviani, M., and F. Porcelli, Nonlinear collisionless magnetic reconnection, *Phys. Rev. Lett.*, *71*, 3802, 1993.

Priest, E.R., *Solar Magnetohydrodynamics*, (Reidel, Dordrecht, 1982).

Priest, E.R. and T. Forbes, Magnetic Reconnection: MHD Theory and Applications (Cambridge University Press, Cambridge, England, 2000).

Pritchett, P. L., Particle-in-Cell simulations of magnetosphere electrodynamics, *IEEE Trans. Plasma Sci.*, 28, 1976, 2000.

Pritchett, P.L., Geospace Environment Modelling magnetic reconnection challenge: Simulation with a full particle electromagnetic code, *J. Geophys. Res.*, 106, 3783, 2001.

Quest, K.B., D.W. Forslund, J.U. Brackbill, and K. Lee, Collisionless dissipation processes in quasi-parallel shocks, *Geophys. Res. Lett.*, 10, 471 (1983).

Ricci, P., G. Lapenta, and J.U. Brackbill, A simplified implicit Maxwell solver, *J. Comp. Phys.*, 183, 117, 2002a.

Ricci, P., G. Lapenta, and J.U. Brackbill, GEM reconnection challenge: implicit kinetic simulations with the physical mass ratio, *Geophys. Res. Lett.*, 29(23), 2008, 10.1029/2002GL015314, 2002b.

Ricci, P., G. Lapenta, and J.U. Brackbill, Electron acceleration and heating in collisionless magnetic reconnection, *Phys. Plasmas*, 10, 3554, 2003.

Rogers, B.N., R.E. Denton, J.F. Drake, and M.A. Shay, Role of dispersive waves in collisionless magnetic reconnection, *Phys. Rev. Lett.*, 87, 195004, 2001.

Rogers, B.N., R.E. Denton, and J.F. Drake, Signatures of collisionless magnetic reconnection, *J. Geophys. Res.*, 108, 1111, 2003.

Romanova, M.M., and R.V.E. Lovelace, Magnetic-field, reconnection, and particle-acceleration in extragalactic jets, *Astron. Astrophys.*, 262, 26, 1992.

Shay, M.A., and J.F. Drake, The role of electron dissipation on the rate of collisionless reconnection, *Geophys. Res. Lett.*, 25, 3759, 1998.

Shay, M. A., J. F. Drake, B.N. Rogers, and R. E. Denton, Alfvénic collisionless magnetic reconnection and the Hall term, *J. Geophys. Res.*, *106*, 3759, 2001.

Sonnerup, B.U.O., Magnetic Field Reconnection, in *Solar System Plasma Physics*, vol. III, edited by L.T. Lanzerotti, C.F. Kennel, and E.N. Parker, p. 45, North-Holland, New York, 1979.

Taylor, J.B., Relaxation and magnetic reconnection in plasmas, *Rev. Mod. Phys.*, *28*, 243, 1986.

Terasawa, T., Hall current effect on tearing mode instability, *Geophys. Res. Lett.*, *10*, 475, 1983.

Vu, H. X. and J. U. Brackbill, CELEST1D: An implicit, fully kinetic model for low-frequency Electromagnetic plasma simulation, *Comput. Phys. Commun.*, *69*, 253, 1992.

Vu, H. X. and J. U. Brackbill, Electron kinetic effects in switch-off slow shocks, *J. Geophys. Res.*, *20*, 2015, 1993.

Wang., X., A. Bhattacharjee, and Z.W. Ma, Collisionless reconnection: effects of Hall current and electron pressure gradient, *J. Geophys. Res.*, *105*, 27633, 2000.

Yamada, M., Review of controlled laboratory experiments on physics of magnetic reconnection, *J. Geophys. Res.*, *104*, 14529, 1999.

Yin, L., and D. Winske, Plasma pressure tensor effects on reconnection: hybrid and Hall-magnetohydrodynamics simulations, *Phys. Plasmas*, *10*, 1595, 2003.

• Fig. 1: The reconnected flux is plotted for $m_i/m_e = 25$ and $B_{y0} = 0$ (a), $m_i/m_e = 25$ and $B_{y0} = B_0$ (b), $m_i/m_e = 25$ and $B_{y0} = 5B_0$ (c), $m_i/m_e = 180$ and $B_{y0} = 0$ (d), $m_i/m_e = 180$ and $B_{y0} = B_0$ (e), $m_i/m_e = 180$ and $B_{y0} = 5B_0$ (f), $m_i/m_e = 1836$ and $B_{y0} = 0$ (g), $m_i/m_e = 1836$ and $B_{y0} = B_0$ (h), and $m_i/m_e = 1836$ and $B_{y0} = 5B_0$ (i). The reconnected flux is normalized to $B_0 c / \omega_{pi}$. The results from CELESTE3D (solid line) and NPIC (dashed) are plotted.

• Fig. 2: For $m_i/m_e = 25$, results from NPIC are shown for the non-ideal part of the reconnection electric field, $E_y + (v_{ze}B_x - v_{xe}B_z)/c$, (a,c,e) and electron pressure contribution to the electric field (b,d,f), $-1/en_e(\partial P_{xye}/\partial y + \partial P_{zye}/\partial z)$. Both plots are color coded, and normalized to $B_0 V_A/c$. The magnetic field lines are plotted in all frames and the guide fields are $B_{y0} = 0$ (a,b), $B_{y0} = B_0$ (c,d), and $B_{y0} = 5B_0$ (e,f). E_y is normalized to $B_0 v_A/c$. The results are plotted at a time when $\Delta\Psi = 1$. The data are averaged over 100 time slices separated by 10 time intervals with $\Delta t \omega_{pi} = 0.014$.

• Fig. 3: The corresponding results to Fig. 2 from CELESTE3D are shown. The data is averaged over a moving window of 100 time steps, with $\Delta t \omega_{pi} = 0.03$.

• Fig. 4: Contributions to the non-ideal reconnection electric field $E_y + (v_{ze}B_x - v_{xe}B_z)/c$ (normalized to $B_0 V_A/c$) (a) given by electron pressure terms, $(\partial P_{xye}/\partial y + \partial P_{zye}/\partial z)$ (b); $v_{xe}\partial v_{ye}/\partial x + v_{ze}\partial v_{ye}/\partial z$ (c), and by all the inertia terms, evaluated as the difference between the non-ideal electric field and the pressure contribution. We consider $m_i/m_e = 25$, $B_{y0} = 5B_0$. The results are plotted at a time when $\Delta\Psi = 1$. These results are from NPIC, and represent average over 100 time slices separated each other by a time step $\Delta t \omega_{pi} = 0.14$.

- Fig. 5: The actual off-diagonal terms of the electron pressure tensor from the NPIC simulation with $m_i/m_e = 25$ and $B_{y0} = 5B_0$ are plotted. Shown are P_{xye} (a), and P_{zye} (c), and their values computed from Eqs. (8) (b), and (9) (d). The results are plotted at a time when $\Delta\Psi = 1$. The data is averaged over 100 time slices separated by a time step $\Delta t\omega_{pi} = 0.14$.

- Fig. 6: Ion (a) and electron (b) motion in the (x, z) plane is shown for $m_i/m_e = 25$ and $B_{y0} = B_0$. The results are plotted at a time when $\Delta\Psi = 1$. These results are from CELESTE3D.

- Fig. 7: Ion (a) and electron (b) motion in the (x, z) plane is shown for $m_i/m_e = 25$ and $B_{y0} = 5B_0$. The results are plotted at a time when $\Delta\Psi = 1$. These results are from CELESTE3D.

- Fig. 8: The electron velocity, v_{ye} , is shown at a time when $\Delta\Psi = 1$, for $B_{y0} = 0$ (a,b), $B_{y0} = B_0$ (c,d), $B_{y0} = 5B_0$ (e,f), and mass ratio $m_i/m_e = 25$. These results are from CELESTE3D (a,c,e) and NPIC (b,d,f).

- Fig. 9: The magnetic field, B_y , is shown when $\Delta\Psi = 1$, for $B_{y0} = 0$ (a,b), $B_{y0} = B_0$ (c,d), $B_{y0} = 5B_0$ (e,f), and mass ratio $m_i/m_e = 25$ (a,c,e), $m_i/m_e = 1836$ (b,d,f). These results are from CELESTE3D.

- Fig. 10: The ion velocity, v_{xi} , is plotted when $\Delta\Psi = 1$, for $B_{y0} = 0$ (a,b), $B_{y0} = B_0$ (c,d), $B_{y0} = 5B_0$ (e,f), and mass ratio $m_i/m_e = 25$ (a,c,e), $m_i/m_e = 1836$ (b,d,f). These results are from CELESTE3D.

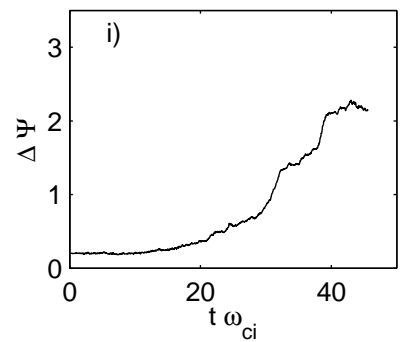
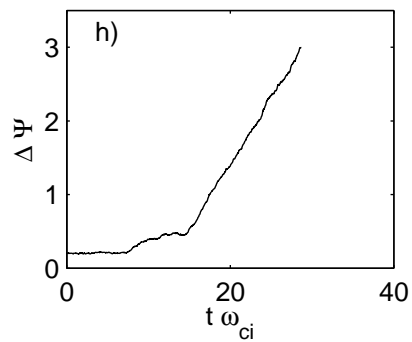
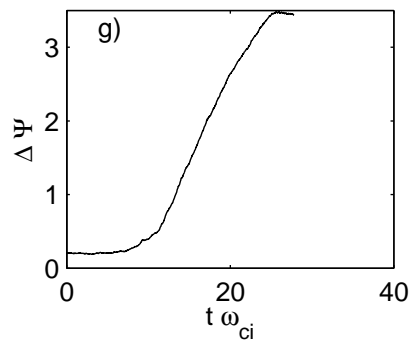
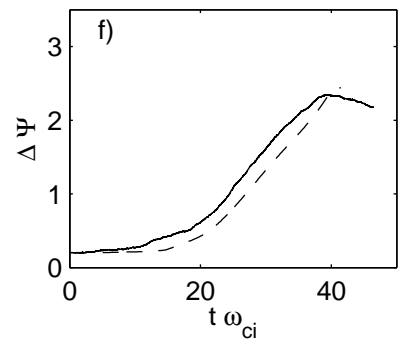
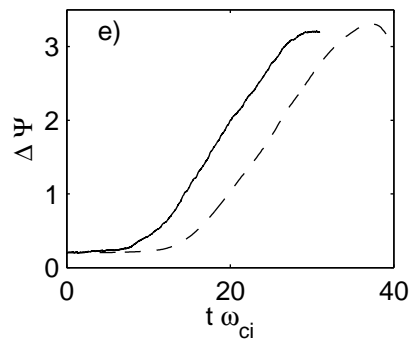
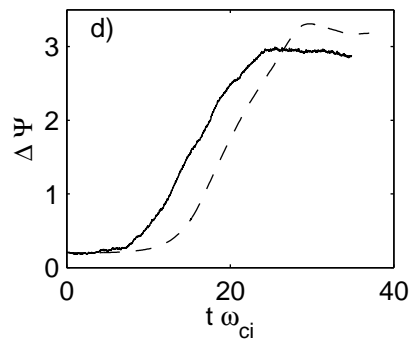
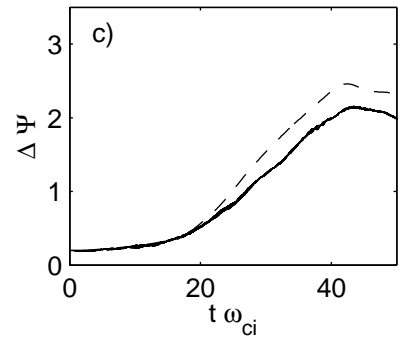
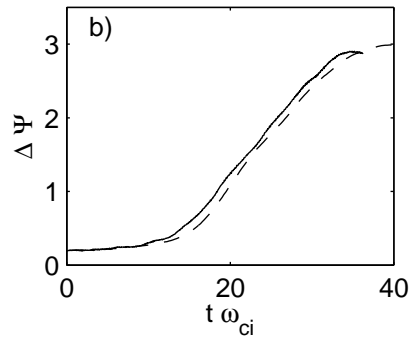
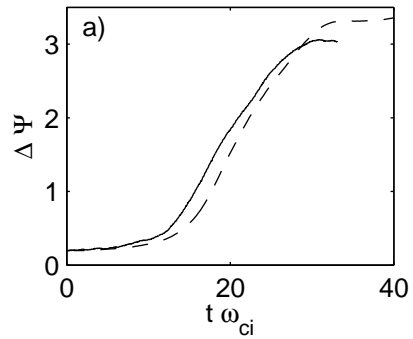
- Fig. 11: The electron density, n_e , is plotted for $m_i/m_e = 25$ and $B_{y0} = 5B_0$ at time $t\omega_{ci} = 30$ in the reconnection region. The results are from CELESTE3D (a) and NPIC (b).

Table I. Decrease of the error in the energy conservation, $\Delta E(t) = [E_{tot}(t) - E_{tot}(0)]/E_{tot}(0)$, at time $t\omega_{ci} = 40$ when the time step is reduced. We consider a set of simulations with $m_i/m_e = 25$, $B_y/B_{y0} = 5$, 64×64 grid points, and 200 particles per cell.

$\Delta t\omega_{pi}$	ΔE
0.30	0.232
0.15	0.076
0.08	0.034
0.03	0.019
explicit (0.014)	$5.6 \cdot 10^{-4}$

Table II. Averaged reconnection rates, normalized to $B_0 v_A/c$, as a function of the guide field and the mass ratio.

	$m_i/m_e = 25$	$m_i/m_e = 180$	$m_i/m_e = 1836$
$B_{y0}/B_0=0$	0.179	0.190	0.206
$B_{y0}/B_0=1$	0.141	0.164	0.182
$B_{y0}/B_0=5$	0.086	0.098	0.113



This figure "fig2.JPG" is available in "JPG" format from:

<http://arxiv.org/ps/astro-ph/0304224v2>

This figure "fig3.JPG" is available in "JPG" format from:

<http://arxiv.org/ps/astro-ph/0304224v2>

This figure "fig4.JPG" is available in "JPG" format from:

<http://arxiv.org/ps/astro-ph/0304224v2>

This figure "fig5.JPG" is available in "JPG" format from:

<http://arxiv.org/ps/astro-ph/0304224v2>

This figure "fig6.jpg" is available in "jpg" format from:

<http://arxiv.org/ps/astro-ph/0304224v2>

This figure "fig7.jpeg" is available in "jpeg" format from:

<http://arxiv.org/ps/astro-ph/0304224v2>

This figure "fig8.JPG" is available in "JPG" format from:

<http://arxiv.org/ps/astro-ph/0304224v2>

This figure "fig9.JPG" is available in "JPG" format from:

<http://arxiv.org/ps/astro-ph/0304224v2>

This figure "fig10.JPG" is available in "JPG" format from:

<http://arxiv.org/ps/astro-ph/0304224v2>

This figure "fig11.JPG" is available in "JPG" format from:

<http://arxiv.org/ps/astro-ph/0304224v2>